Structural Dynamics ARTICLE pubs.aip.org/aip/sdy

First experiments with ultrashort, circularly polarized soft x-ray pulses at FLASH2

Cite as: Struct. Dyn. **12**, 034301 (2025); doi: 10.1063/4.0000298
Submitted: 31 January 2025 · Accepted: 24 April 2025 ·
Published Online: 8 May 2025

S. Marotzke,[1,2] D. Gupta,[3] R.-P. Wang,[1] M. Pavelka,[4] S. Dziarzhytski,[1] C. von Korff Schmising,[5] S. Jana,[5] N. Thielemann-Kühn,[6] T. Amrhein,[6] M. Weinelt,[6] I. Vaskivskyi,[7] R. Knut,[4] D. Engel,[5] M. Braune,[1] M. Ilchen,[1,8,9] S. Savio,[8,10] T. Otto,[1,8] K. Tiedtke,[1] V. Scheppe,[3,6] J. Rönsch-Schulenberg,[1] E. Schneidmiller,[1] C. Schüßler-Langeheine,[3] H. A. Dürr,[4] M. Beye,[1,11] G. Brenner,[1] and N. Pontius[3,a)]

AFFILIATIONS

[1]Deutsches Elektronen-Synchrotron DESY, Notkestraße 85, 22607 Hamburg, Germany
[2]Institut für Experimentelle und Angewandte Physik, Christian-Albrechts-Universität zu Kiel, Olshausenstr. 40, 24098 Kiel, Germany
[3]Helmholtz-Zentrum Berlin für Materialien und Energie, Albert-Einstein-Str. 15, 12489 Berlin, Germany
[4]Department of Physics and Astronomy, Uppsala University, Box 256, 751 05 Uppsala, Sweden
[5]Max Born Institute for Nonlinear Optics and Short Pulse Spectroscopy, Max-Born Straße 2A, 12489 Berlin, Germany
[6]Freie Universität Berlin, Fachbereich Physik, Arnimallee 14, 14195 Berlin, Germany
[7]J. Stefan Institute, Jamova cesta 39, 1000 Ljubljana, Slovenia
[8]Universität Hamburg, Luruper Chaussee 149, 22761 Hamburg, Germany
[9]Center for Free-Electron Laser Science CFEL, Deutsches Elektronen-Synchrotron DESY, Notkestraße 85, 22607 Hamburg, Germany
[10]Technische Universität Dortmund, Maria-Goeppert-Mayer-Straße 2, 44227 Dortmund, Germany
[11]Stockholm University, SE-106 91 Stockholm, Sweden

Note: This paper is part of the Special Topic Celebrating the work and the achievements of Jo Stöhr.
[a)]**Author to whom correspondence should be addressed:** pontius@helmholtz-berlin.de

ABSTRACT

Time-resolved absorption spectroscopy and magnetic circular dichroism with circularly polarized soft x-rays (XAS and XMCD) are powerful tools to probe electronic and magnetic dynamics in magnetic materials element- and site-selectively. By employing these methods, groundbreaking results have been obtained, for instance, for magnetic alloys, which helped to fundamentally advance the field of ultrafast magnetization dynamics. At the free-electron laser facility FLASH, key capabilities for ultrafast XAS and XMCD experiments have recently improved. In an upgrade, an APPLE-III helical afterburner undulator was installed at FLASH2 in September 2023. This installation allows for the generation of circularly polarized soft x-ray pulses with a duration of a few tens of femtoseconds covering the $L_{3,2}$-edges of the important 3*d* transition metal elements with pulse energies of several μJ. Here, we present first experimental results with such ultrashort x-ray pulses from the FL23 beamline employing XMCD at the $L_{3,2}$-edges of the 3*d* metals, Co, Fe, and Ni. We obtain significant dichroic difference signals indicating a degree of circular polarization close to 100%. With the pulse-length preserving monochromator at beamline FL23 and an improved pump-laser setup, FLASH can offer important and efficient experimental instrumentation for ultrafast demagnetization studies and other investigations of ultrafast spin dynamics in 3*d* transition metals, multilayers, and alloys.

I. INTRODUCTION

Soft x-ray based resonant methods have provided one of the biggest contributions to the fundamental understanding of ultrafast magnetization dynamics in multi-element materials since the emergence of the field.[1] The importance hinges on the inherent element specificity of soft x-ray resonances, their sensitivity to the atomic magnetic state, the ability to analyze dissipation of individual spin and orbital moments that determine the materials' magnetization,[2–10] and even the possibility to obtain spatially resolved information.[11,12] These experimental results have significantly advanced the field of magnetization dynamics research.

Soft x-ray methods are element-specific since they probe resonant electronic transitions from localized atomic core levels to valence states. The resonances appear at characteristic, well-separated energies for each element. The sensitivity to the atomic magnetic properties, i.e., spin and orbital momenta, is essentially based on the effect of x-ray Magnetic Circular Dichroism (XMCD):[13] the difference in absorption of circularly polarized x-rays of opposite helicity (i.e., photon angular momenta of $+1\,\hbar$ or $-1\,\hbar$). Selection rules govern the spin-conserving resonant optical transition from a spin–orbit coupled core state into the spin-specific density of valence states induced by the magnetic order. This leads to a helicity-dependent absorption strength. The so-called sum rules can be derived for XMCD spectra, allowing for the determination of the absolute atomic orbital and spin magnetic moments for individual elements as well as their dynamic changes.[13–15]

The crucial requirement for ultrafast dynamics studies with the above-mentioned methods is the availability of circularly polarized ultrashort soft x-ray pulses. First, groundbreaking contributions allowed for fundamentally new insights into the ultrafast magnetization dynamics and have already been made by a storage ring based source starting in 2007.[2–10] Electron bunch slicing was used in combination with an Apple-II type undulator for the generation of circularly polarized soft x-ray radiation at the BESSY II Femtoslicing source.[16] Nowadays, free-electron lasers (FELs) are capable of providing intense x-ray pulses of a few to a few tens of femtoseconds duration or even below. Oftentimes though, the experimental temporal resolution is rather limited by the pulse duration of external pump lasers and the employed synchronization and jitter correction schemes.

While free-electron laser facilities produce short wavelength radiation since 2005[17] and soft x-rays since 2009,[18] soft x-rays were initially provided only with linear polarization; ultrashort circularly polarized soft x-ray pulses were produced significantly later at these facilities.[19]

The first FEL based experiments using ultrashort circularly polarized soft x-ray pulses have been reported at the LCLS in 2016.[20,21] In 2023, first lasing results with circular polarization at the soft x-ray FEL beamline Athos of SwissFEL were published.[22,23] At the FERMI facility ultrashort pulses with circular polarization in the VUV, employing an APPLE-II type undulator was already available since the inception,[24] complementary to laser-based high-harmonic generation (HHG) lab sources;[25,26] the generation of elliptically polarized femtosecond pulses in a seeded operation mode at the $L_{3,2}$-edges of magnetic transition metals (700–800 eV) though has only been demonstrated at FERMI recently.[27] At EuXFEL (SA3), an APPLE X (UE90) undulator for ultrashort x-ray pulse generation with variable polarization has recently entered user operation.[28]

The increasing number of FEL facilities providing circularly polarized soft x-ray pulses offers new possibilities for ultrafast dynamics studies on magnetic materials. FEL sources have the potential for femtosecond temporal and sub-eV energetic resolutions combined with high x-ray intensities for high fidelity studies. In this contribution, we report on the first experiments with ultrashort circularly polarized soft x-ray pulses at FLASH2 in the photon energy range from 700 to 860 eV. We measured XMCD spectra of the $L_{3,2}$-edges of the magnetic transition metals Fe, Co, and the L_3-edge of Ni using circularly polarized x-ray pulses from the recently implemented afterburner undulator.[29]

The availability of circular polarization at the FLASH facility opens up the possibility to extend the available experimental time for soft x-ray methods based ultrafast magnetization dynamics studies. The future potential of ultrafast experiments with circularly polarized x-ray pulses on the elemental magnets Fe, Co, and Ni even goes beyond the analytical tools that have been discussed so far. Recent studies on the Co-L_3 edge demonstrate new insight into the ultrafast occupation changes within the *spin-dependent* density of states, governing the magnetic dynamics at different times and timescales.[9,30]

II. THE FLASH AFTERBURNER AND RADIATION DIAGNOSTICS

The measurements reported here were carried out at the XUV/soft x-ray free-electron laser FLASH at DESY in Hamburg. FLASH, as a user facility, serves FEL radiation to two different experimental halls.[17,31] The common FLASH linear accelerator consists of a normal-conducting radio frequency-gun, superconducting electron acceleration modules, including a third harmonic cavity, two bunch compressors, and a laser heater system. It is capable of generating bunch trains with several thousand electron bunches per second in 10 Hz bursts of up to 800 μs length. The electron bunches can reach beam energies up to 1.35 GeV and peak currents of up to a few kA. A beam distribution yard, based on a kicker and a septum magnet, enables the parallel operation of the two undulator beamlines called FLASH1 and FLASH2. The bunch trains can be divided into two variable parts with slightly different properties.

The FLASH2 undulator beamline contains 12 planar, variable gap undulators, each 2.5 m long. Downstream from these planar undulators, an APPLE-III type afterburner undulator was installed at the end of September 2023.[29] The afterburner undulator allows for the generation of FEL radiation with variable polarization at the third harmonic of the FLASH2 SASE FEL radiation, i.e., down to 1.33 nm, corresponding to 930 eV photon energy. The parameter settings of FLASH2 for the present measurements are given in Table I.

The afterburner can be tuned to produce differently polarized x-ray pulses (including circular left and right). The main challenge in operating this device is the strong linearly polarized background from the main FLASH2 undulator that would contaminate the desired photon polarization state. A method for suppression of such a background was proposed in Ref. 32: an application of the reverse undulator taper. The main effect of this technique is that the radiation is strongly suppressed, while the microbunching at the exit of the main undulator is practically the same as in the reference case of the non-tapered undulator. Then, the micro-bunched beam emits powerful radiation with required polarization properties in the afterburner. This method was successfully used to operate the helical afterburner at LCLS.[19]

Since the APPLE-III afterburner at FLASH2 is operated at the third harmonic of the main undulator, the reverse taper method is employed to suppress mostly the weaker linearly polarized radiation at the third harmonic, which worked very well during the experiment and provided high purity circularly polarized photons. The fundamental from the main undulator was also suppressed, although less efficiently than the third harmonic. The remaining fundamental radiation was then filtered out in the beamline monochromator, which was used to select the third harmonic. This allowed for optimization of the afterburner settings and the experiment itself. In addition to applying a reverse taper, a modification of the electron optics at the end of the undulator line was introduced in order to improve the electron beam focusing into the afterburner, thus increasing the radiation intensity and polarization purity.

TABLE I. Overview of the technical parameters of FLASH2 and the pump-laser used in the present experiment.

Parameter	FLASH2	Optical laser
Macro-train repetition rate	10 Hz	10 Hz
Intra-train repetition rate (spacing)	1 MHz (1 μs)	100 kHz (10 μs)
No. of micro-pulses	400	80 (40 used)
Train duration	400 μs	800 μs (400 μs used)
Wavelength	1.44–1.78 nm	1030 nm
Photon energy	700–860 eV	1.2 eV
Electron beam energy	1360 MeV	n.a.
Electron bunch charge	340 pC	n.a.
Approx. spot size on sample	$\sim 12 \times 36\ \mu m^2$	$\sim 175 \times 225\ \mu m^2$
FL23 beamline resolution[a]	800 meV (single grating mode)	

[a]By design, the FL23 monochromator has an $E/\Delta E$ resolution of 1500.

The FEL radiation generated with these undulator schemes was characterized by photon-diagnostics measurements during the commissioning of the afterburner undulator prior to the experiment presented here. In this characterization study, we used an instrument comprising a set of circularly arranged photoelectron time-of-flight (TOF) spectrometers to measure the angular distribution of photoelectrons emitted from atomic gas targets in the plane perpendicular to the FEL beam propagation.[33] In the dipole approximation for a one-photon ionization process, the angular intensity distribution I depending on the polar angle θ in the detection plane can be described by

$$I(\theta) = \frac{\sigma}{4\pi}\left[1 + \frac{\beta}{4}[1 + 3 \cdot P_{\mathrm{lin}} \cdot \cos(2(\theta - \psi))]\right]. \quad (1)$$

Here, σ and β are the cross section and the anisotropy parameter, respectively, for the ionization of the particular electronic subshell of the target gas, P_{lin} is the degree of linear polarization, and ψ is the angle of the linear polarization direction with respect to the horizontal axis, i.e., $\psi = 0$ represents horizontal linear polarization. While the linear polarization is usually characterized by the Stokes-Poincaré parameters S_1 and S_2, P_{lin} and ψ constitute an alternative representation:[34]

$$P_{\mathrm{lin}} = \sqrt{S_1^2 + S_2^2}, \quad \tan(2\psi) = \frac{S_2}{S_1}. \quad (2)$$

From Eq. (1), it is obvious that with this kind of experimental setup, only the linear polarization component of the FEL radiation can be measured directly. In fact, the circular polarization component $P_{\mathrm{circ}} = S_3$ corresponds to an isotropic angular distribution pattern, which, in principle, cannot be distinguished from unpolarized radiation. However, for FELs, one can assume almost perfect polarization with a negligible unpolarized component fraction on the order of the Pierce parameter $\rho \approx 10^{-3}$.[35] Hence, the degree of circular polarization can be determined without being able to differentiate between right and left helicity by

$$P_{\mathrm{circ}} = \sqrt{1 - P_{\mathrm{lin}}^2}. \quad (3)$$

The capability of this method has been successfully demonstrated previously for different undulator types and polarization setup schemes at FERMI and LCLS.[19,20,36–38]

For the afterburner-undulator characterization at FLASH, we used rare gases as ionization targets. Values of ionization cross section σ and angular distribution anisotropy parameters β for the addressed electronic states of these gases, which are needed for reference, can be found in the literature over a wide range of photon energies. Photoelectron angular distribution measurements have been performed for different linear and circular polarization settings of the afterburner undulator at various photon energies of the third harmonic in the range from 74 to 414 eV. Details about the commissioning campaign will be published elsewhere.

As an example, in Fig. 1, we present the angular distribution patterns measured at 313.8 eV of the FEL's third harmonic for three different afterburner undulator settings corresponding to the horizontal linear, vertical linear, and circular polarization. The derived values P_{lin} for both linear polarization settings derived from this acquisition dataset are $P_{\mathrm{lin}}^{\mathrm{h}} = 0.96 \pm 0.02$ and $P_{\mathrm{lin}}^{\mathrm{v}} = 0.98 \pm 0.02$, whereas for circular polarization $P_{\mathrm{lin}}^{\mathrm{c}} = 0.07 \pm 0.02$. The uncertainty of 2% is the error of the weighted mean of the results using different methods for the photoelectron yield determination, which we applied as a test for a robust analysis procedure suited for a fast diagnostics tool. With a more conservative error estimation, the deduced value of the degree of circular polarization of the third harmonic at 313.8 eV is $P_{\mathrm{circ}} = 99.7\ ^{+0.3}_{-0.4}\%$.

III. EXPERIMENTAL SETUP

In the present measurements, FLASH2 was tuned for the third harmonic radiation to reach the Co and Fe $L_{3,2}$ and the Ni L_3-edges. Employing the FLASH2 afterburner undulator (see Sec. II), circularly polarized photons were generated delivering 400 FEL-laser pulses per train. The train repetition rate was 10 Hz, and the intra-train pulse repetition rate was 1 MHz (i.e., 1 μs single pulse time spacing, total pulse train duration 400 μs; compare also Table I).

The XMCD experiment was carried out at the monochromator beamline FL23[40] of the FLASH2 FEL facility[17,31] employing the MUSIX (multidimensional spectroscopy and inelastic x-ray scattering) endstation,[41,42] see Fig. 2. Two 3 mm iris apertures were used upstream of FL23 to constrain the beam path. The beamline was operated in first-order single-diffraction grating mode to select the third harmonic radiation, using the high-energy grating with a groove density of 600 lines/mm and an energy dispersion of 0.017 nm/mm in the energy range 700–860 eV. An exit slit of 100 μm width led to an energy

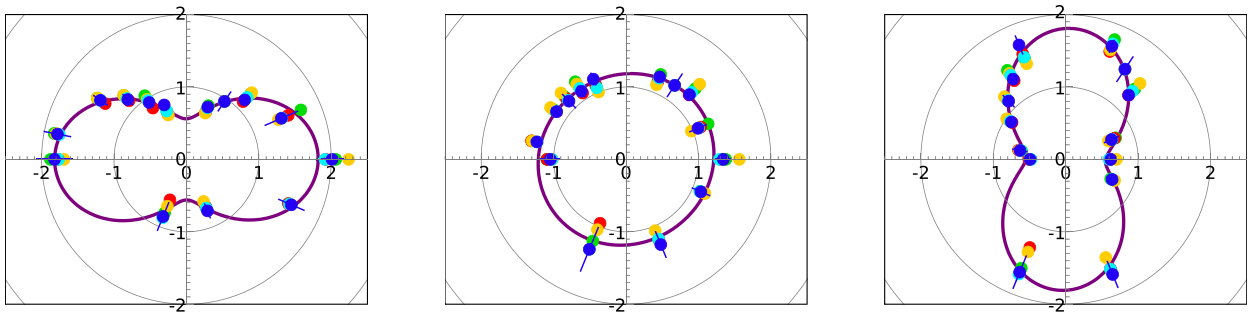

FIG. 1. Angular distribution patterns of ionization of Kr 3*d* at $h\nu_{3rd} = 313.8$ eV for different polarization modes of the FLASH2 afterburner undulator: linear horizontal (left), circular (mid), and linear vertical (right). The circles represent the measured Kr, 3*d* photoline intensity for each eTOF, and its corresponding angle in the dipole plane. The colors of the circles refer to different methods to determine the photoelectron signal intensity in the TOF spectrum: photoline profile fit (dark blue), raw intensity integration in an ROI around the photoline with different background definitions (light blue, yellow, and green), and photoline amplitude values (red). The purple line represents the angular distribution according to Eq. (1), with the weighted mean values for P_{lin} and ψ.

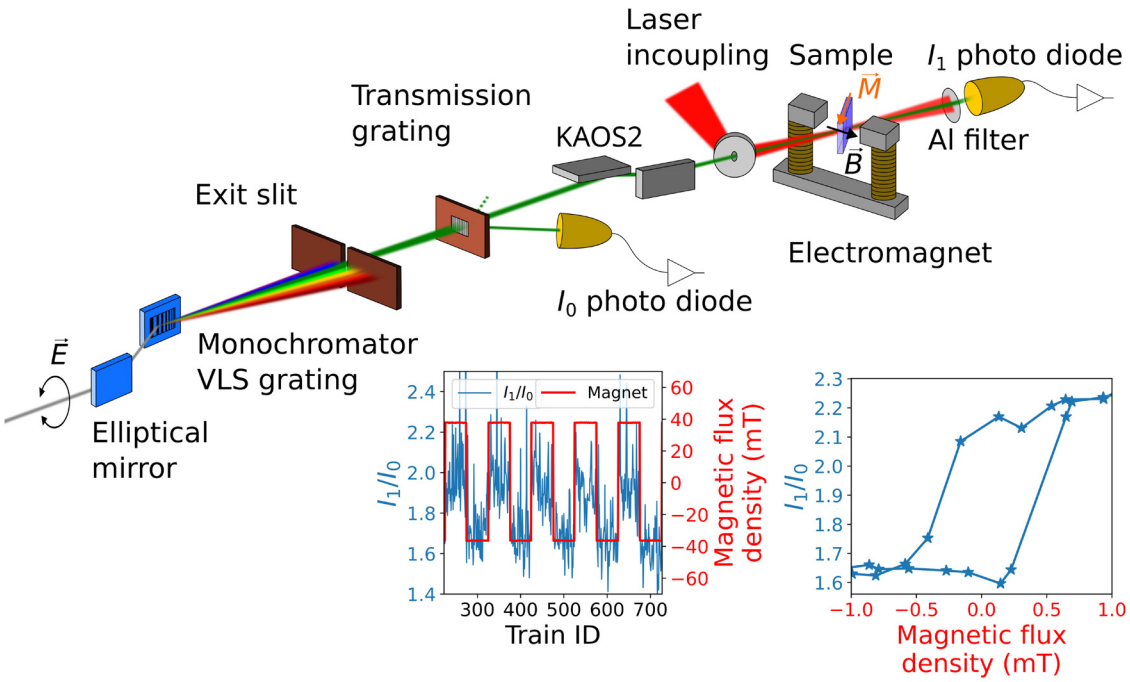

FIG. 2. Sketch of the experimental setup. The new FLASH2 helical afterburner undulator enables full polarization control in the photon energy range of the magnetic 3*d* transition metal $L_{3,2}$-edges. For this study, the beamline was operated in a single-diffraction grating mode. A transmission grating behind the monochromator exit slit enables a split-beam normalization scheme for intensity normalization of shot-to-shot SASE fluctuations. Focusing of the x-ray beam is achieved by a Kirkpatrick-Baez active optics system (KAOS2).[39] The MUSIX endstation with an in-vacuum electromagnet together with a co-linear laser in-coupling allows for time-resolved XMCD measurements. The right hand inset shows a static hysteresis of the FeNi sample at the Fe L_3-edge; the left hand inset shows representatively the continuously alternating magnetic field together with the recorded normalized transmission signal within a 100 s interval of data acquisition.

resolution of approximately 800 meV. In order to maximize the beamline transmission, the coatings of all beamline optics were either set to Ni (Fe and Co $L_{3,2}$-edge) or Pt (Ni L_3-edge). The first diffraction order of a transmission grating placed after the middle slit of the first FL23 monochromator was detected by a photo diode to act as monitor of the incidence x-ray intensity I_0, while the zeroth order was guided further towards the sample.[43,44] The transmission grating consists of a 100 nm Si_3N_4 membrane on which grating lines made from a HSQ (hydrogen silsesquioxane) resist with a height of >200 nm, a duty cycle of 0.5, and a grating period of 320 nm are fabricated. For the zeroth order, a focusing Kirkpatrick-Baez active optics system (KAOS2) was used to focus the beam onto the FeNi or CoPt sample to a transversal spot size of $12 \times 36\ \mu m^2$. The intensity I_1 of the transmitted beam was measured with a second biased photo diode. The signals of both x-ray

photo diodes were measured for every individual x-ray pulse enabling normalization on a shot-to-shot basis. To avoid saturation of the photo diode during the measurements at the Fe $L_{3,2}$-edge, a 197 nm Nb filter was inserted into the beamline while at the Ni L_3-edge, the gas attenuator (Krypton) was used at 1.5×10^{-2} mbar to further attenuate the fundamental.

To excite the sample in the time-resolved measurements, a fixed time-structure pulse train of 80 optical laser pulses (1030 nm) at a frequency of 100 kHz (i.e., 10 μs pulse spacing; pulse train duration 800 μs) and a train repetition rate of 10 Hz was provided. Since the optical laser pulse train showed an almost linear pulse energy build-up for the first 20 pulses before reaching a constant pulse energy level, the delay to the x-ray pulse trains was set such that the first FEL pulse in a train overlapped with laser pulse 21. Due to the different repetition rates of FEL (1 MHz) and optical laser pulses (100 kHz), every tenth FEL pulse was temporally overlapped with an optical pump-laser pulse, such that a total of 40 FEL pulses of a pulse train could be used for the time-resolved measurements. The pulse energy of the optical laser pulses was varied by combining two sets of neutral density filters in the beam path. The spot size of the optical laser on the sample was separately determined by knife-edge scans (see Table I) and substantially larger than that of the FEL beam. Spatial overlap of laser and FEL spots was verified by a Ce-doped YAG based fluorescence crystal (imaged with a long-working distance microscope and a CCD camera) at the sample position. The BAM (beam arrival monitor, measuring the electron beam timing relative to a master clock) and the LAM (laser arrival monitor, referencing the laser pulses to the same master clock) were used to correct the data for jitter and drifts between FEL and pump laser.[45–47]

The x-ray absorption spectra of the Fe, Co $L_{3,2}$, and Ni L_3-edges (L_2 corresponding to the $2p_{1/2} \rightarrow 3d$, and L_3 to the $2p_{3/2} \rightarrow 3d$ transitions) were obtained by simultaneously moving the gap of the planar undulators and the helical afterburner together with the monochromator pitch angle. For the XMCD measurements, the x-ray beam transmitted through the samples at 35° - 45° with respect to the sample normal, and their magnetization was flipped horizontally in the sample plane by an external magnetic field (see Fig. 2). The latter was generated by an in-vacuum electromagnet, which is able to generate a maximum magnetic field of approximately 100 mT. Magnetic saturation of the samples was ensured by applying a magnetic field of $\pm$ 36 mT, exceeding the saturation field of the sample (see the exemplary hysteresis scan for the FeNi sample in Fig. 2). During the measurements, the magnetic field direction was inverted every 10 s. The helicity of the FEL beam was kept fixed for all measurements.

The samples were grown by magnetron sputtering at the Max Born Institute Berlin. The substrates were Si frames (Silson Ltd.) with 15 Si_3N_4 windows of 0.5×0.5 mm^2 lateral size. The layer structure of the CoPt sample was Al(100 nm)/SiN(200 nm)/Ta(2 nm)/$Co_{50}Pt_{50}$(25 nm)/MgO(2 nm), and that of the FeNi sample was Al(100 nm)/SiN(200 nm)/Ta(2 nm)/$Fe_{40}Ni_{60}$(25 nm)/MgO(2 nm). The Al layer served as a heat sink and the MgO layer as protection against oxidation.

For analyzing the degree of x-ray polarization at FLASH2, reference XMCD measurements were done after the FLASH2 studies on the identical samples at the PM3 beamline of the BESSY II storage ring.[48]

IV. EXPERIMENTAL RESULTS

Symbols in Figs. 3(a)–3(f) show static XAS and XMCD spectra of the $L_{3,2}$-edge photon energy region of Fe, Co, and Ni measured at FLASH2. XAS spectra for opposite magnetic field orientation (black and red) are presented in plots (a)–(c). The spectra were calculated from the acquired raw data as

$$T(E) = \frac{I_1}{I_0}, \tag{4}$$

$$\mathrm{XAS}(E) = \log\left(\frac{T(E)}{T(E < L_3)}\right) \cdot \cos(\vartheta), \tag{5}$$

$$\mathrm{XMCD}(E) = \left(\mathrm{XAS}^{M+}(E) - \mathrm{XAS}^{M-}(E)\right) / \sin(\vartheta). \tag{6}$$

Here, $T(E)$ is the sample transmitted intensity signal (diode signal I_1) normalized to I_0 (monitor diode signal) on a shot-to-shot basis. For proper normalization, events with almost vanishing I_0 values were discarded. The such obtained x-ray transmission spectra, $T(E)$, were normalized to the signal level in the photon energy range (few eV) immediately below the L_3 resonance, denoted as $E < L_3$. The logarithm of the normalized transmission spectra then scales with the x-ray absorption coefficient of the $L_{3,2}$-edge optical transitions.[13] For the different resonances, we tuned the angles of incidence, ϑ, to optimize both the transmission signal by changing the effective sample thickness, hence the value of absorption, and the XMCD amplitude determined by the projection angle of the in-plane sample magnetization onto the x-ray k-vector. In order to compensate for different absorption of various angles of incidence, the XAS spectra were multiplied by the factor $\cos(\vartheta)$. These XAS spectra are shown in Figs. 3(a)–3(c) for Fe, Co, and Ni, respectively. The net acquisition time for one pair of XAS spectra (M+ and M−) was between 3 and 4 h. Note that in this early stage of the afterburner operation, the accelerator tuning was optimized for a single energy close to the $L_{3,2}$-resonances, which, in part, led to dramatic intensity drops in photon energy regions far from the tuning energy, such as in the high-energy tails of the spectra. At these low intensities, the normalization to the reference I_0 turned out to be less reliable. Moreover, for Ni, only the L_3 absorption edge could be measured, as the L_2 absorption edge energy was beyond the limits of the FLASH2 accelerator setting in this first measurement campaign.

The XMCD spectra are calculated by subtracting both spectra, $\mathrm{XAS}^{M+}(E)$ and $\mathrm{XAS}^{M-}(E)$, recorded for opposite magnetic field directions. To correct for the different projections of the sample magnetization onto the x-ray direction of individual measurements, the XMCD spectra are divided by the factor $\sin(\vartheta)$ [see Eq. (6)].[13] Hence, all XMCD spectra are scaled to the unified configuration with the magnetic field vector parallel to the x-ray direction. The resulting XMCD spectra for Fe, Co, and Ni are shown in Figs. 3(d)–3(f) (open blue circles), respectively. All elements show significant XMCD.

We compare these spectra with reference spectra taken from the identical samples at the PM3 beamline of the BESSY II storage ring [see Figs. 3(g)–3(i)].[48] The latter are derived from the raw data in the same way as those recorded at FLASH2; here, I_1 is the photo-current of a photo diode detecting the sample transmitted intensity, and I_0 is the corresponding signal measured without any sample (incident intensity). For proper comparison, we have to consider that the XMCD spectra for FeNi have been recorded at different temperatures (PM3: 295 K; FL23: 80 K). The lower temperature for the FL23 measurements results in a slightly larger saturation magnetization, hence an increased XMCD. Referring to temperature-dependent studies on similar samples from literature,[49] we find an ∼8% larger magnetization for FeNi at 80 K, which we assume to directly translate into the

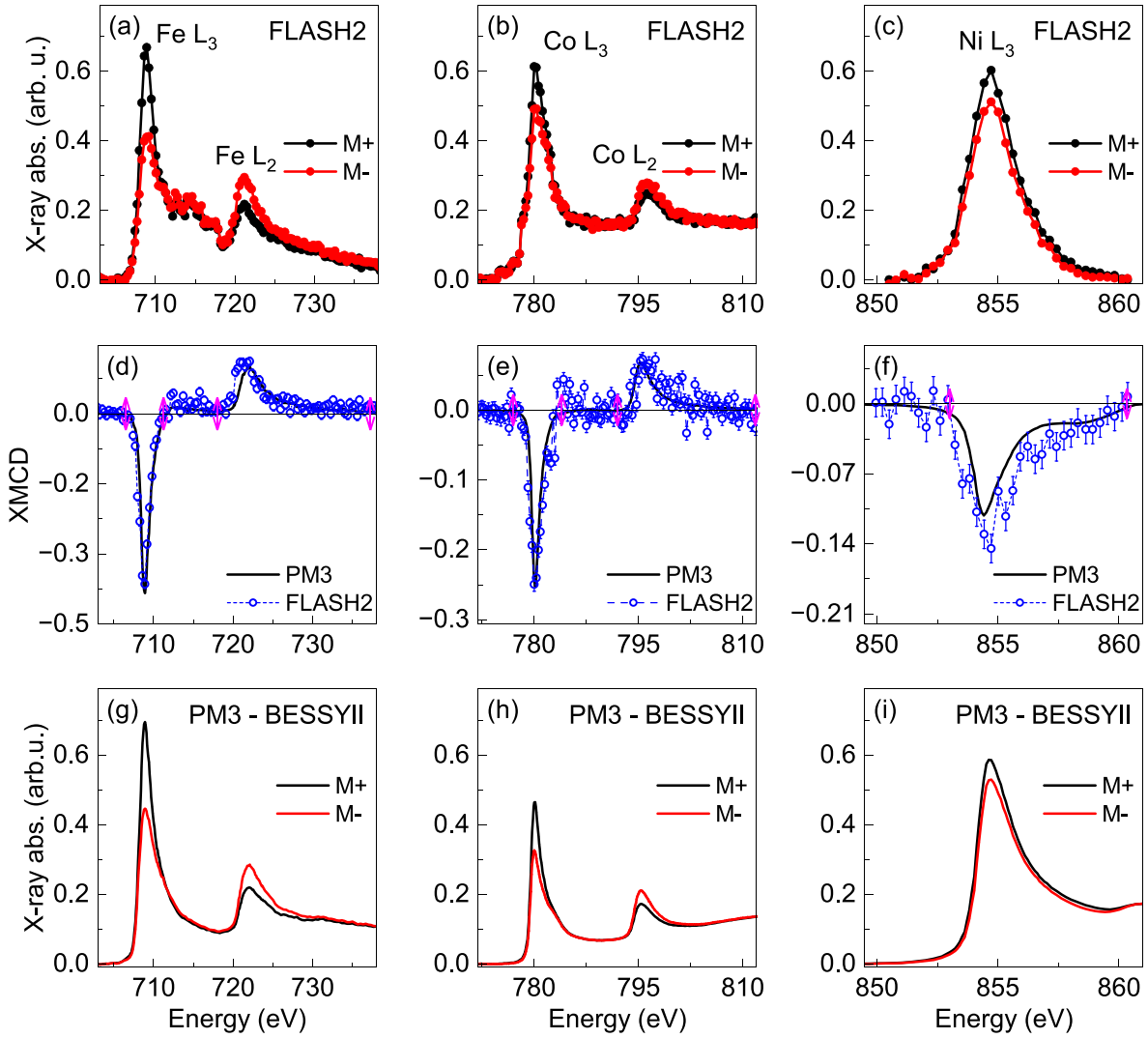

FIG. 3. Static XAS and XMCD spectra at the Fe, Co, and Ni *L*-edge: (a)–(c) show XAS spectra recorded at the FL23 beamline of FLASH2 with circularly polarized x-ray pulses. For Ni, only the L_3 absorption resonance is shown up to 860 eV, which was the upper photon energy limit of the FLASH2 accelerator during this first measurement campaign. (g)–(i) XAS spectra of the same samples taken for reference at the BESSY II storage ring. (d)–(f) The XMCD spectra derived from the corresponding XAS spectra. The pink arrows indicate the integration limits for the comparison of the absolute value of XMCD in the FL23 and PM3 measurements (see the text).

XMCD amplitude. This factor is considered in the comparison of the FLASH2 spectra and their PM3 reference spectra in Figs. 3(g)–3(i).

We notice that the spectral shape differs between the FL23 and PM3 data, in particular in the background regions on the high-energy sides of the Fe and Ni L_2 peaks. The FL23 data also show jumps, e.g., in the low-energy slope of the Co L_3 or Fe L_2 peaks. We assign these to the imperfect normalization mentioned earlier.

Since the imperfect normalization mostly affects the energy regions further away from the absorption maxima, where the XMCD mostly vanishes, we expect that with some limitations, the XMCD signal allows us to estimate the degree of circular polarization. For this, we use the known degree of circular polarization for the PM3 measurements[48,50] and the unified representation of all XMCD spectra. To correct for the different energy resolution of the two monochromators (FL23: 800 meV; PM3: 300 meV), we integrate the XMCD spectra over the individual $L_{3,2}$-resonances. The absolute values of this integration are shown in Table II for each resonance (row $XMCD_{PM3}$ and $XMCD_{FL23}$).

For the PM3 reference measurements, the degree of the x-ray circular polarization (S_3, Stokes–Poincaré parameter) has been experimentally determined or extrapolated from an experimentally determined value (see Table II).[48,50] Since the samples are identical, and the spectra have been normalized to a unified measuring condition, the XMCD values determined for FL23 allow an assessment of S_3 for the FLASH2 measurements by scaling the PM3 S_3 value by the ratio $XMCD_{FL23}/XMCD_{PM3}$. The such obtained S_3 values of the

TABLE II. The table comprises the absolute values of the energy integration over the XMCD $L_{3,2}$-resonances of Fe, Co, and Ni for the spectra measured at PM3 (row $XMCD_{PM3}$) and FL23 (row $XMCD_{FL23}$), given in arbitrary units [compare Figs. 3(d)–3(f) and see text for details]. The experimental errors given for the $XMCD_{FL23}$ values are purely statistical, calculated by error progression from the mean error of the XMCD spectra data points; they do not include systematic errors caused by imperfect normalization. The corresponding statistical experimental errors for $XMCD_{PM3}$ are negligible and, therefore, not shown. For the PM3 measurements, the experimentally determined degree of circular polarization, S_3, for the respective absorption edges is given underneath the integration numbers.[48,50] S_3 for FL23 is estimated by scaling the PM3 value by the experimentally determined ratio of the integrated XMCD values of the individual resonances. See text for the experimental errors of the $S3$ values.

	Fe L_3	Fe L_2	Co L_3	Co L_2	Ni L_3
$XMCD_{PM3}$	0.66	0.57	0.42	0.28	0.26
S_3 (%)	92.5	92.5	92.7	92.8	93.0
$XMCD_{FL23}$	0.69 ± 0.05	0.67 ± 0.09	0.54 ± 0.04	0.26 ± 0.08	0.39 ± 0.07
S_3 (%)	97^{+3}_{-7}	100^{+0}_{-14}	100^{+0}_{-9}	86^{+14}_{-26}	100^{+0}_{-25}

FLASH2 circular polarization for the individual L-resonance energies are given in the bottom row of Table II. We note that for Fe L_2, Co L_3, and Ni L_3, the scaling results in mean values and even uncertainty intervals are greater than 100%. We assign this to the imperfect normalization of the FL23 data mentioned earlier, which leads to additional uncertainties not included in the error bars for $XMCD_{FL23}$; the latter only describe the scatter in spectra. We, therefore, capped the values and error bars given in Table II at 100%; the negative uncertainties are those of the uncapped values.

Essentially, we find S_3 values consistent with almost 100% circular polarization as expected. The apparently small value for Co L_2 of 86% is probably due to the relatively large experimental error (see earlier). The differing values for Co L_3 and L_2, however, could as well stem from a non-synchronous gap change of the Apple-III afterburner and the main FLASH2 undulator during the energy scans. This is a matter of undulator parameters calibration and will be improved in the future.

To demonstrate the feasibility of ultrafast dynamics magnetic studies with circular polarization, we present the ultrafast element specific XMCD transient of Fe in the FeNi sample after laser excitation. Due to the 20 laser pulses in each pulse train, which arrived before the first pulse of the FEL pulse train (intensity build-up, see Sec. III), a considerable nearly constant heating of the samples was observed leading to a significant reduction of the sample base magnetization and XMCD. Even liquid nitrogen cooling of the samples could not remove this effect. Yet, a compromise had to be found for the pump-laser fluence, minimizing the heating while dynamically inducing a significant demagnetization.

The effective temporal resolution of this measurement results from various contributions (see Table III): the laser and the x-ray pulse widths and the jitter/drift in the FEL-laser synchronization. The latter contributions can partially be corrected for by measurements of BAM and LAM (see Sec. III). Additional temporal broadening can arise from the beamline monochromator, which was used in the single grating mode. Here, the x-ray pulse elongation depends on how many grating grooves are illuminated by the x-ray beam and can vary between 100 and 200 fs depending on the beamline alignment. Summing up all the contributions, the temporal resolution for our experiment was expected to be in a range between 170 and 270 fs.

Figure 4 displays the transient XMCD of Fe in the FeNi sample. This alloy typically shows a demagnetization time constant of ∼250 fs for Fe in FeNi depending on the excitation strength and the sample design.[10,51–53] Since the time constant is known, the measured transient XMCD allows us to experimentally verify the temporal resolution under the present conditions. We fitted the transient XMCD with the following function:

$$F(t) = G(t,\Delta\tau) * \left(C_0 + C_1 \cdot H(t-t_0) \cdot \left(1 - \exp^{-(t-t_0)/\tau_d}\right) \cdot \exp^{-(t-t_0)/\tau_r}\right). \tag{7}$$

Here, a double exponential function, which mimics the magnetic dynamics, is convolved with a Gaussian function, $G(t,\Delta\tau)$, taking into account the experimental time resolution $\Delta\tau$ (FWHM). τ_d is the time constant for the demagnetization, and τ_r is a second time constant modeling the recovery. t_0 denotes the time of simultaneous arrival of pump and probe pulse. $H(t-t_0)$ is the Heaviside function ($H(t-t_0) = 0$ if $t < t_0$ and $H(t-t_0) = 1$ if $t > t_0$).

Except the demagnetization time, τ_d, which was kept fixed at 250 fs, we left all other parameters free in the fitting process. This yields a time resolution $\Delta\tau$ of 150 ± 30 fs, which overlaps with the lower limit of the temporal resolution estimated earlier.

TABLE III. Overview of the parameters of FLASH2 and the pump laser determining the effective temporal resolution during the present beamtime. The parameters enter the temporal resolution in different manners (see footnotes). The BAM allows us to correct the train-to-train jitter from the data. The shot-to-shot jitter/drift of the single x-ray pulses within the train (30 fs) was not corrected in the present measurement and fully enters the effective temporal resolution. BAM correction leaves a remaining broadening of the train-to-train jitter less than 10 fs. Without the elongation by the monochromator, an effective temporal resolution of 90 fs would result.

Parameter	Value
Laser pulse width[a]	∼75 fs
X-ray pulse width[a]	∼30 fs
Remaining jitter after BAM correction[a,b]	≤10 fs
- train-to-train arrival time jitter/drift	55 fs
- intra-train shot-to-shot arrival time jitter/drift	30 fs
Remaining drifts after LAM correction[a]	≤35 fs
X-ray pulse elongation by monochromator[c]	≤200 fs
Effective experimental time resolution	≤270 fs

[a]Enters effective time resolution by convolution.
[b]Only train-to-train jitter is corrected.
[c]Enters effective time resolution by summation.

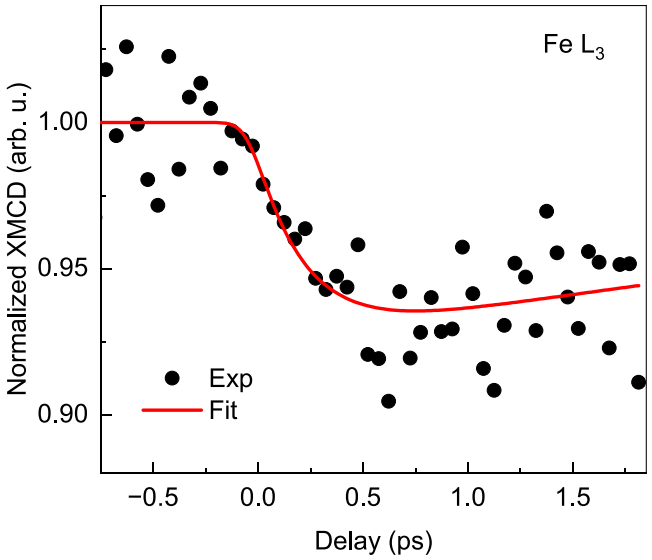

FIG. 4. Normalized transient demagnetization dynamics of Fe in FeNi measured at the Fe L_3 absorption resonance (black circles). The solid red line represents the exponential fit with Gaussian convolution.

V. CONCLUSIONS

We have successfully used ultrashort circularly polarized soft x-ray pulses at the FLASH2 facility in the photon energy range 700–860 eV. The degree of circular polarization is found to be consistent with almost 100%. This photon energy range covers the $L_{3,2}$-edges of the 3*d* elemental magnets Fe and Co and the L_3-edge of Ni, which are highly relevant for the field of ultrafast magnetization dynamics. After further accelerator commissioning, the available photon energy range will also cover the Ni L_2-edge (870 eV). With the envisaged improvements to the pump-laser system to make the pulse energies in the train more uniform, a higher repetition rate pump laser, and improved overall temporal resolution, FLASH will offer even more interesting research possibilities for ultrafast spin dynamics experiments on 3*d* transition metals.

ACKNOWLEDGMENTS

We acknowledge DESY (Hamburg, Germany), a member of the Helmholtz Association HGF, for the provision of experimental facilities. Parts of this research were carried out at the beamline FL23 at FLASH2. Beamtime was allocated for proposals F-20211728 EC and F-20220710. The statics reference measurements were carried out at the PM3 scattering instrument at the BESSY II electron storage ring operated by the Helmholtz-Zentrum Berlin für Materialien und Energie; we would like to thank Torsten Kachel for the experimental support. This work was supported by the Deutsche Forschungsgemeinschaft (DFG) through TRR 227 "Ultrafast Spin Dynamics," Project ID 328545488 (projects A01, A02, and A03) and by the Bundesministerium für Bildung und Forschung (BMBF) through the project "Spinflash" (05K22KE2).

AUTHOR DECLARATIONS

Conflict of Interest

The authors have no conflicts to disclose.

Author Contributions

S. Marotzke: Formal analysis (equal); Investigation (equal); Methodology (equal); Software (equal); Visualization (equal); Writing – original draft (equal); Writing – review & editing (equal). **D. Gupta:** Formal analysis (equal); Investigation (equal); Visualization (equal); Writing – original draft (equal); Writing – review & editing (equal). **R.-P. Wang:** Formal analysis (equal); Investigation (equal); Methodology (equal); Software (equal); Writing – review & editing (equal). **M. Pavelka:** Investigation (equal); Writing – review & editing (equal). **S. Dziarzhytski:** Investigation (equal); Methodology (equal); Writing – review & editing (equal). **C. von Korff Schmising:** Conceptualization (equal); Investigation (equal); Resources (equal); Writing – review & editing (equal). **S. Jana:** Formal analysis (equal); Investigation (equal); Writing – review & editing (equal). **N. Thielemann-Kühn:** Formal analysis (equal); Investigation (equal); Writing – review & editing (equal). **T. Amrhein:** Formal analysis (equal); Investigation (equal); Writing – review & editing (equal). **M. Weinelt:** Funding acquisition (equal); Investigation (equal); Writing – review & editing (equal). **I. Vaskivskyi:** Formal analysis (equal); Investigation (equal); Writing – review & editing (equal). **R. Knut:** Investigation (equal); Writing – review & editing (equal). **D. Engel:** Resources (lead); Writing – review & editing (equal). **M. Braune:** Methodology (equal); Writing – original draft (equal); Writing – review & editing (equal). **M. Ilchen:** Methodology (equal); Writing – review & editing (equal). **S. Savio:** Methodology (equal); Writing – review & editing (equal). **T. Otto:** Methodology (equal); Writing – review & editing (equal). **K. Tiedtke:** Methodology (equal); Writing – review & editing (equal). **V. Scheppe:** Methodology (equal); Writing – review & editing (equal). **J. Rönsch-Schulenberg:** Methodology (equal); Writing – review & editing (equal). **E. Schneidmiller:** Investigation (equal); Methodology (equal); Writing – original draft (equal); Writing – review & editing (equal). **C. Schüßler-Langeheine:** Conceptualization (equal); Funding acquisition (equal); Investigation (equal); Methodology (equal); Supervision (equal); Writing – review & editing (equal). **H. A. Dürr:** Investigation (equal); Writing – review & editing (equal). **M. Beye:** Conceptualization (equal); Formal analysis (equal); Investigation (equal). Methodology (equal); Project administration (equal); Software (equal); Writing – review & editing (equal). **G. Brenner:** Conceptualization (equal); Investigation (equal); Methodology (equal); Project administration (equal); Visualization (equal); Writing – original draft (equal); Writing – review & editing (equal). **N. Pontius:** Conceptualization (lead); Funding acquisition (equal); Investigation (equal); Methodology (equal); Project administration (equal); Supervision (equal); Visualization (equal); Writing – original draft (lead); Writing – review & editing (equal).

DATA AVAILABILITY

The data that support the findings of this study are openly available in Zenodo at https://doi.org/10.5281/zenodo.15076836, Ref. 54.

REFERENCES

[1]E. Beaurepaire, J.-C. Merle, A. Daunois, and J.-Y. Bigot, "Ultrafast spin dynamics in ferromagnetic nickel," Phys. Rev. Lett. **76**, 4250 (1996).
[2]C. Stamm, T. Kachel, N. Pontius, R. Mitzner, T. Quast, K. Holldack, S. Khan, C. Lupulescu, E. F. Aziz, M. Wietstruk, H. A. Dürr, and W. Eberhardt,

"Femtosecond modification of electron localization and transfer of angular momentum in nickel," Nat. Mater. **6**, 740 (2007).
[3]C. Boeglin, E. Beaurepaire, V. Halté, V. López-Flores, C. Stamm, N. Pontius, H. A. Dürr, and J.-Y. Bigot, "Distinguishing the ultrafast dynamics of spin and orbital moments in solids," Nature **465**, 458 (2010).
[4]I. Radu, K. Vahaplar, C. Stamm, T. Kachel, N. Pontius, H. Dürr, T. Ostler, J. Barker, R. F. L. Evans, R. W. Chantrell, A. Tsukamoto, A. Itoh, A. Kirilyuk, T. Rasing, and A. V. Kimel, "Transient ferromagnetic-like state mediating ultrafast reversal of antiferromagnetically coupled spins," Nature **472**, 205 (2011).
[5]M. Wietstruk, A. Melnikov, C. Stamm, T. Kachel, N. Pontius, M. Sultan, C. Gahl, M. Weinelt, H. A. Dürr, and U. Bovensiepen, "Hot-electron-driven enhancement of spin-lattice coupling in Gd and Tb 4*f* ferromagnets observed by femtosecond x-ray magnetic circular dichroism," Phys. Rev. Lett. **106**, 127401 (2011).
[6]A. Eschenlohr, M. Battiato, P. Maldonado, N. Pontius, T. Kachel, K. Holldack, R. Mitzner, A. Föhlisch, P. M. Oppeneer, and C. Stamm, "Ultrafast spin transport as key to femtosecond demagnetization," Nat. Mater. **12**, 332 (2013).
[7]M. Hennecke, I. Radu, R. Abrudan, T. Kachel, K. Holldack, R. Mitzner, A. Tsukamoto, and S. Eisebitt, "Angular momentum flow during ultrafast demagnetization of a ferrimagnet," Phys. Rev. Lett. **122**, 157202 (2019).
[8]E. Golias, I. Kumberg, I. Gelen, S. Thakur, J. Gördes, R. Hosseinifar, Q. Guillet, J. Dewhurst, S. Sharma, C. Schuler-Langeheine, N. Pontius, and W. Kuch, "Ultrafast optically induced ferromagnetic state in an elemental antiferromagnet," Phys. Rev. Lett. **126**, 107202 (2021).
[9]L. Le Guyader, D. J. Higley, M. Pancaldi, T. Liu, Z. Chen, T. Chase, P. W. Granitzka, G. Coslovich, A. A. Lutman, G. L. Dakovski, W. F. Schlotter, P. Shafer, E. Arenholz, O. Hellwig, M. L. M. Lalieu, B. Koopmans, A. H. Reid, S. Bonetti, J. Stöhr, and H. A. Dürr, "State-resolved ultrafast charge and spin dynamics in [Co/Pd] multilayers," Appl. Phys. Lett. **120**, 032401 (2022).
[10]S. Jana, R. Knut, S. Muralidhar, R. Malik, R. Stefanuik, J. Åkerman, O. Karis, C. Schüßler-Langeheine, and N. Pontius, "Experimental confirmation of the delayed Ni demagnetization in FeNi alloy," Appl. Phys. Lett. **120**, 102404 (2022).
[11]C. E. Graves, A. H. Reid, T. Wang, B. Wu, S. de Jong, K. Vahaplar, I. Radu, D. P. Bernstein, M. Messerschmidt, L. Müller, R. Coffee, M. Bionta, S. W. Epp, R. Hartmann, N. Kimmel, G. Hauser, A. Hartmann, P. Holl, H. Gorke, J. H. Mentink, A. Tsukamoto, A. Fognini, J. J. Turner, W. F. Schlotter, D. Rolles, H. Soltau, L. Strüder, Y. Acremann, A. V. Kimel, A. Kirilyuk, T. Rasing, J. Stöhr, A. O. Scherz, and H. A. Dürr, "Nanoscale spin reversal by non-local angular momentum transfer following ultrafast laser excitation in ferrimagnetic GdFeCo," Nat. Mater. **12**, 293 (2013).
[12]E. Iacocca, T.-M. Liu, A. H. Reid, Z. Fu, S. Ruta, P. W. Granitzka, E. Jal, S. Bonetti, A. X. Gray, C. E. Graves, R. Kukreja, Z. Chen, D. J. Higley, T. Chase, L. Le Guyader, K. Hirsch, H. Ohldag, W. F. Schlotter, G. L. Dakovski, G. Coslovich, M. C. Hoffmann, S. Carron, A. Tsukamoto, A. Kirilyuk, A. V. Kimel, T. Rasing, J. Stöhr, R. F. L. Evans, T. Ostler, R. W. Chantrell, M. A. Hoefer, T. J. Silva, and H. A. Dürr, "Spin-current-mediated rapid magnon localisation and coalescence after ultrafast optical pumping of ferrimagnetic alloys," Nat. Commun. **10**, 1756 (2019).
[13]J. Stöhr, H. C. Siegmann, J. Stöhr, and H. C. Siegmann, *Magnetism* (Springer, Berlin, Heidelberg, 2006), Vol. 152.
[14]B. T. Thole, P. Carra, F. Sette, and G. van der Laan, "X-ray circular dichroism as a probe of orbital magnetization," Phys. Rev. Lett. **68**, 1943 (1992).
[15]P. Carra, B. T. Thole, M. Altarelli, and X. Wang, "X-ray circular dichroism and local magnetic fields," Phys. Rev. Lett. **70**, 694 (1993).
[16]K. Holldack, J. Bahrdt, A. Balzer, U. Bovensiepen, M. Brzhezinskaya, A. Erko, A. Eschenlohr, R. Follath, A. Firsov, W. Frentrup, L. Le Guyader, T. Kachel, P. Kuske, R. Mitzner, R. Müller, N. Pontius, T. Quast, I. Radu, J.-S. Schmidt, C. Schüßler-Langeheine, M. Sperling, C. Stamm, C. Trabant, and A. Föhlisch, "FemtoSpeX: A versatile optical pump–soft X-ray probe facility with 100 fs X-ray pulses of variable polarization," J. Synchrotron Rad. **21**, 1090 (2014).
[17]W. Ackermann, G. Asova, V. Ayvazyan, A. Azima, N. Baboi, J. Bähr, V. Balandin, B. Beutner, A. Brandt, A. Bolzmann, R. Brinkmann, O. I. Brovko, M. Castellano, P. Castro, L. Catani, E. Chiadroni, S. Choroba, A. Cianchi, J. T. Costello, D. Cubaynes, J. Dardis, W. Decking, H. Delsim-Hashemi, A. Delserieys, G. Di Pirro, M. Dohlus, S. Düsterer, A. Eckhardt, H. T. Edwards, B. Faatz, J. Feldhaus, K. Flöttmann, J. Frisch, L. Fröhlich, T. Garvey, U. Gensch, C. Gerth, M. Görler, N. Golubeva, H.-J. Grabosch, M. Grecki, O. Grimm, K. Hacker, U. Hahn, J. H. Han, K. Honkavaara, T. Hott, M. Hüning, Y. Ivanisenko, E. Jaeschke, W. Jalmuzna, T. Jezynski, R. Kammering, V. Katalev, K. Kavanagh, E. T. Kennedy, S. Khodyachykh, K. Klose, V. Kocharyan, M. Körfer, M. Kollewe, W. Koprek, S. Korepanov, D. Kostin, M. Krassilnikov, G. Kube, M. Kuhlmann, C. L. S. Lewis, L. Lilje, T. Limberg, D. Lipka, F. Löhl, H. Luna, M. Luong, M. Martins, M. Meyer, P. Michelato, V. Miltchev, W. D. Möller, L. Monaco, W. F. O. Müller, O. Napieralski, O. Napoly, P. Nicolosi, D. Nölle, T. Nuñez, A. Oppelt, C. Pagani, R. Paparella, N. Pchalek, J. Pedregosa-Gutierrez, B. Petersen, B. Petrosyan, G. Petrosyan, L. Petrosyan, J. Pflüger, E. Plönjes, L. Poletto, K. Pozniak, E. Prat, D. Proch, P. Pucyk, P. Radcliffe, H. Redlin, K. Rehlich, M. Richter, M. Roehrs, J. Roensch, R. Romaniuk, M. Ross, J. Rossbach, V. Rybnikov, M. Sachwitz, E. L. Saldin, W. Sandner, H. Schlarb, B. Schmidt, M. Schmitz, P. Schmüser, J. R. Schneider, E. A. Schneidmiller, S. Schnepp, S. Schreiber, M. Seidel, D. Sertore, A. V. Shabunov, C. Simon, S. Simrock, E. Sombrowski, A. A. Sorokin, P. Spanknebel, R. Spesyvtsev, L. Staykov, B. Steffen, F. Stephan, F. Stulle, H. Thom, K. Tiedtke, M. Tischer, S. Toleikis, R. Treusch, D. Trines, I. Tsakov, E. Vogel, T. Weiland, H. Weise, M. Wellhöfer, M. Wendt, I. Will, A. Winter, K. Wittenburg, W. Wurth, P. Yeates, M. V. Yurkov, I. Zagorodnov, and K. Zapfe, "Operation of a free-electron laser from the extreme ultraviolet to the water window," Nat. Photonics **1**, 336 (2007).
[18]P. Emma, R. Akre, J. Arthur, R. Bionta, C. Bostedt, J. Bozek, A. Brachmann, P. Bucksbaum, R. Coffee, F.-J. Decker, Y. Ding, D. Dowell, S. Edstrom, A. Fisher, J. Frisch, S. Gilevich, J. Hastings, G. Hays, P. Hering, Z. Huang, R. Iverson, H. Loos, M. Messerschmidt, A. Miahnahri, S. Moeller, H.-D. Nuhn, G. Pile, D. Ratner, J. Rzepiela, D. Schultz, T. Smith, P. Stefan, H. Tompkins, J. Turner, J. Welch, W. White, J. Wu, G. Yocky, and J. Galayda, "First lasing and operation of an Ångstrom-wavelength free-electron laser," Nat. Photonics **4**, 641 (2010).
[19]A. A. Lutman, J. P. MacArthur, M. Ilchen, A. O. Lindahl, J. Buck, R. N. Coffee, G. L. Dakovski, L. Dammann, Y. Ding, H. A. Dürr, L. Glaser, J. Grünert, G. Hartmann, N. Hartmann, D. Higley, K. Hirsch, Y. I. Levashov, A. Marinelli, T. Maxwell, A. Mitra, S. Moeller, T. Osipov, F. Peters, M. Planas, I. Shevchuk, W. F. Schlotter, F. Scholz, J. Seltmann, J. Viefhaus, P. Walter, Z. R. Wolf, Z. Huang, and H.-D. Nuhn, "Polarization control in an X-ray free-electron laser," Nat. Photonics **10**, 468 (2016).
[20]G. Hartmann, A. O. Lindahl, A. Knie, N. Hartmann, A. A. Lutman, J. P. MacArthur, I. Shevchuk, J. Buck, A. Galler, J. M. Glownia, W. Helml, Z. Huang, N. M. Kabachnik, A. K. Kazansky, J. Liu, A. Marinelli, T. Mazza, H.-D. Nuhn, P. Walter, J. Viefhaus, M. Meyer, S. Moeller, R. N. Coffee, and M. Ilchen, "Circular dichroism measurements at an x-ray free-electron laser with polarization control," Rev. Sci. Instrum. **87**, 083113 (2016).
[21]D. J. Higley, K. Hirsch, G. L. Dakovski, E. Jal, E. Yuan, T. Liu, A. A. Lutman, J. P. MacArthur, E. Arenholz, Z. Chen, G. Coslovich, P. Denes, P. W. Granitzka, P. Hart, M. C. Hoffmann, J. Joseph, L. Le Guyader, A. Mitra, S. Moeller, H. Ohldag, M. Seaberg, P. Shafer, J. Stöhr, A. Tsukamoto, H.-D. Nuhn, A. H. Reid, H. A. Dürr, and W. F. Schlotter, "Femtosecond X-ray magnetic circular dichroism absorption spectroscopy at an X-ray free electron laser," Rev. Sci. Instrum. **87**, 033110 (2016).
[22]E. Prat, A. Al Haddad, C. Arrell, S. Augustin, M. Boll, C. Bostedt, M. Calvi, A. L. Cavalieri, P. Craievich, A. Dax, P. Dijkstal, E. Ferrari, R. Follath, R. Ganter, Z. Geng, N. Hiller, M. Huppert, R. Ischebeck, P. Juranić, C. Kittel, G. Knopp, A. Malyzhenkov, F. Marcellini, S. Neppl, S. Reiche, N. Sammut, T. Schietinger, T. Schmidt, K. Schnorr, A. Trisorio, C. Vicario, D. Voulot, G. Wang, and T. Weilbach, "An X-ray free-electron laser with a highly configurable undulator and integrated chicanes for tailored pulse properties," Nat. Commun. **14**, 5069 (2023).
[23]C. Kittel, A. Sarracini, S. Augustin, N. Yang, A. Al Haddad, E. Ferrari, G. Knopp, J. Knurr, A. S. Morillo-Candas, I. Swiderska, E. Prat, N. Sammut, T. Schmidt, C. Bostedt, M. Calvi, and K. Schnorr, "Demonstration of full polarization control of soft X-ray pulses with Apple X undulators at SwissFEL using recoil ion momentum spectroscopy," J. Synchrotron Rad. **31**, 1134 (2024).
[24]E. Allaria, R. Appio, L. Badano, W. Barletta, S. Bassanese, S. Biedron, A. Borga, E. Busetto, D. Castronovo, P. Cinquegrana, S. Cleva, D. Cocco, M. Cornacchia, P. Craievich, I. Cudin, G. D'Auria, M. D. Forno, M. Danailov, R. D. Monte, G. D. Ninno, P. Delgiusto, A. Demidovich, S. D. Mitri, B. Diviacco, A. Fabris, R. Fabris, W. Fawley, M. Ferianis, E. Ferrari, S. Ferry, L. Froehlich, P. Furlan,

G. Gaio, F. Gelmetti, L. Giannessi, M. Giannini, R. Gobessi, R. Ivanov, E. Karantzoulis, M. Lonza, A. Lutman, B. Mahieu, M. Milloch, S. Milton, M. Musardo, I. Nikolov, S. Noe, F. Parmigiani, G. Penco, M. Petronio, L. Pivetta, M. Predonzani, F. Rossi, L. Rumiz, A. Salom, C. Scafuri, C. Serpico, P. Sigalotti, S. Spampinati, C. Spezzani, M. Svandrlik, C. Svetina, S. Tazzari, M. Trovo, R. Umer, A. Vascotto, M. Veronese, R. Visintini, M. Zaccaria, D. Zangrando, and M. Zangrando, "Highly coherent and stable pulses from the FERMI seeded free-electron laser in the extreme ultraviolet," Nat. Photonics **6**, 699 (2012).

[25]O. Kfir, P. Grychtol, E. Turgut, R. Knut, D. Zusin, D. Popmintchev, T. Popmintchev, H. Nembach, J. M. Shaw, A. Fleischer, H. Kapteyn, M. Murnane, and O. Cohen, "Generation of bright phase-matched circularly-polarized extreme ultraviolet high harmonics," Nat. Photonics **9**, 99 (2015).

[26]G. Lambert, B. Vodungbo, J. Gautier, B. Mahieu, V. Malka, S. Sebban, P. Zeitoun, J. Luning, J. Perron, A. Andreev, S. Stremoukhov, F. Ardana-Lamas, A. Dax, C. P. Hauri, A. Sardinha, and M. Fajardo, "Towards enabling femtosecond helicity-dependent spectroscopy with high-harmonic sources," Nat. Commun. **6**, 6167 (2015).

[27]C. Spezzani, A. Ravindran, E. Allaria, L. Badano, R. Bhardwaj, A. Brynes, P. Capaldo, A. Caretta, P. Cinquegrana, A. Contillo, M. Danailov, A. Demidovich, S. Dal Zillo, G. D. Ninno, B. Diviacco, G. Kurdi, D. Garzella, G. Geloni, L. Giannessi, S. Laterza, M. Manfredda, I. Nikolov, M. Pancaldi, M. Pasqualetto, E. Pedersoli, G. Penco, G. Perosa, M. Prica, L. Raimondi, P. Rebernik Ribič, C. Scafuri, P. Sigalotti, A. Simoncig, F. Sottocorona, S. Spampinati, P. Susnjar, F. Tripaldi, M. Trovò, M. Zangrando, F. Capotondi, N. Jaouen, M. Malvestuto, and M. Sacchi, "Circular dichroism experiments at the *L* edge of magnetic transition metals enabled by elliptically polarized pulses from a seeded free-electron laser," Phys. Rev. B **110**, 174409 (2024).

[28]M. Yakopov, M. Calvi, S. Casalbuoni, U. Englisch, S. Karabekyan, X. Liang, and T. Schmidt, "Characterization of helical APPLE X undulators with 90 mm period for the European XFEL," J. Phys. Conf. Ser. **2380**, 012019 (2022).

[29]M. Tischer, H. Bienert, K. Götze, D. Meissner, P. Neumann, P. N'Gotta, T. Ramm, A. Schöps, P. Talkovski, S. Telawane, and P. Vagin, "Development of an APPLE-III undulator for FLASH-2," J. Phys. Conf. Ser. **2380**, 012017 (2022).

[30]N. Pontius, J. K. Dewhurst, C. Schuessler-Langeheine, S. Jana, C. v. Korff Schmising, S. Eisebitt, S. Shallcross, and S. Sharma, "Mapping the energy-time landscape of spins with helical x-rays," arXiv:2205.03172 (2022).

[31]B. Faatz, E. Plönjes, S. Ackermann, A. Agababyan, V. Asgekar, V. Ayvazyan, S. Baark, N. Baboi, V. Balandin, N. V. Bargen, Y. Bican, O. Bilani, J. Bödewadt, M. Böhnert, R. Böspflug, S. Bonfigt, H. Bolz, F. Borges, O. Borkenhagen, M. Brachmanski, M. Braune, A. Brinkmann, O. Brovko, T. Bruns, P. Castro, J. Chen, M. Czwalinna, H. Damker, W. Decking, M. Degenhardt, A. Delfs, T. Delfs, H. Deng, M. Dressel, H.-T. Duhme, S. Düsterer, H. Eckoldt, A. Eislage, M. Felber, J. Feldhaus, P. Gessler, M. Gibau, N. Golubeva, T. Golz, J. Gonschior, A. Grebentsov, M. Grecki, C. Grün, S. Grunewald, K. Hacker, L. Hänisch, A. Hage, T. Hans, E. Hass, A. Hauberg, O. Hensler, M. Hesse, K. Heuck, A. Hidvegi, M. Holz, K. Honkavaara, H. Höppner, A. Ignatenko, J. Jäger, U. Jastrow, R. Kammering, S. Karstensen, A. Kaukher, H. Kay, B. Keil, K. Klose, V. Kocharyan, M. Köpke, M. Körfer, W. Kook, B. Krause, O. Krebs, S. Kreis, F. Krivan, J. Kuhlmann, M. Kuhlmann, G. Kube, T. Laarmann, C. Lechner, S. Lederer, A. Leuschner, D. Liebertz, J. Liebing, A. Liedtke, L. Lilje, T. Limberg, D. Lipka, B. Liu, B. Lorbeer, K. Ludwig, H. Mahn, G. Marinkovic, C. Martens, F. Marutzky, M. Maslocv, D. Meissner, N. Mildner, V. Miltchev, S. Molnar, D. Mross, F. Müller, R. Neumann, P. Neumann, D. Nölle, F. Obier, M. Pelzer, H.-B. Peters, K. Petersen, A. Petrosyan, G. Petrosyan, L. Petrosyan, V. Petrosyan, A. Petrov, S. Pfeiffer, A. Piotrowski, Z. Pisarov, T. Plath, P. Pototzki, M. Prandolini, J. Prenting, G. Priebe, B. Racky, T. Ramm, K. Rehlich, R. Riedel, M. Roggli, M. Röhling, J. Rönsch-Schulenburg, J. Rossbach, V. Rybnikov, J. Schäfer, J. Schaffran, H. Schlarb, G. Schlesselmann, M. Schlösser, P. Schmid, C. Schmidt, F. Schmidt-Föhre, M. Schmitz, E. Schneidmiller, A. Schöps, M. Scholz, S. Schreiber, K. Schütt, U. Schütz, H. Schulte-Schrepping, M. Schulz, A. Shabunov, P. Smirnov, E. Sombrowski, A. Sorokin, B. Sparr, J. Spengler, M. Staack, M. Stadler, C. Stechmann, B. Steffen, N. Stojanovic, V. Sychev, E. Syresin, T. Tanikawa, F. Tavella, N. Tesch, K. Tiedtke, M. Tischer, R. Treusch, S. Tripathi, P. Vagin, P. Vetrov, S. Vilcins, M. Vogt, A. D. Z. Wagner, T. Wamsat, H. Weddig, G. Weichert, H. Weigelt, N. Wentowski, C. Wiebers, T. Wilksen, A. Willner, K. Wittenburg, T. Wohlenberg, J. Wortmann, W. Wurth, M. Yurkov, I. Zagorodnov, and J. Zemella, "Simultaneous operation of two soft x-ray free-electron lasers driven by one linear accelerator," New J. Phys. **18**, 062002 (2016).

[32]E. Schneidmiller and M. Yurkov, "Obtaining high degree of circular polarization at x-ray free electron lasers via a reverse undulator taper," Phys. Rev. Spec. Top. Accel. Beams **16**, 110702 (2013).

[33]M. Braune, G. Hartmann, M. Ilchen, A. Knie, T. Lischke, A. Reinköster, A. Meissner, S. Deinert, L. Glaser, O. Al-Dossary, A. Ehresmann, A. S. Kheifets, and J. Viefhaus, "Electron angular distributions of noble gases in sequential two-photon double ionization," J. Mod. Opt. **63**, 324 (2016).

[34]V. Schmidt, "Photoionization of atoms using synchrotron radiation," Rep. Prog. Phys. **55**, 1483 (1992).

[35]G. Geloni, V. Kocharyan, and E. Saldin, "Theoretical computation of the polarization characteristics of an x-ray free-electron laser with planar undulator," Opt. Commun. **356**, 435 (2015).

[36]E. Allaria, B. Diviacco, C. Callegari, P. Finetti, B. Mahieu, J. Viefhaus, M. Zangrando, G. De Ninno, G. Lambert, E. Ferrari, J. Buck, M. Ilchen, B. Vodungbo, N. Mahne, C. Svetina, C. Spezzani, S. Di Mitri, G. Penco, M. Trovó, W. M. Fawley, P. R. Rebernik, D. Gauthier, C. Grazioli, M. Coreno, B. Ressel, A. Kivimäki, T. Mazza, L. Glaser, F. Scholz, J. Seltmann, P. Gessler, J. Grünert, A. De Fanis, M. Meyer, A. Knie, S. P. Moeller, L. Raimondi, F. Capotondi, E. Pedersoli, O. Plekan, M. B. Danailov, A. Demidovich, I. Nikolov, A. Abrami, J. Gautier, J. Lüning, P. Zeitoun, and L. Giannessi, "Control of the polarization of a vacuum-ultraviolet, high-gain, free-electron laser," Phys. Rev. X **4**, 041040 (2014).

[37]E. Ferrari, E. Allaria, J. Buck, G. De Ninno, B. Diviacco, D. Gauthier, L. Giannessi, L. Glaser, Z. Huang, M. Ilchen, G. Lambert, A. A. Lutman, B. Mahieu, G. Penco, C. Spezzani, and J. Viefhaus, "Single shot polarization characterization of XUV FEL pulses from crossed polarized undulators," Sci. Rep. **5**, 13531 (2015).

[38]C. von Korff Schmising, D. Weder, T. Noll, B. Pfau, M. Hennecke, C. Strüber, I. Radu, M. Schneider, S. Staeck, C. M. Günther, J. Lüning, A. e d Merhe, J. Buck, G. Hartmann, J. Viefhaus, R. Treusch, and S. Eisebitt, "Generating circularly polarized radiation in the extreme ultraviolet spectral range at the free-electron laser FLASH," Rev. Sci. Instrum. **88**, 053903 (2017).

[39]P. Kirkpatrick and A. V. Baez, "Formation of optical images by x-rays," J. Opt. Soc. Am. **38**, 766 (1948).

[40]L. Poletto, F. Frassetto, G. Brenner, M. Kuhlmann, and E. Plönjes, "Double-grating monochromatic beamline with ultrafast response for FLASH2 at DESY," J. Synchrotron Rad. **25**, 131 (2018).

[41]The MUSIX end station is ready for users; experimental requirements should be discussed with the scientists in charge.

[42]M. Beye, R. Y. Engel, J. O. Schunck, S. Dziarzhytski, G. Brenner, and P. S. Miedema, "Non-linear soft x-ray methods on solids with MUSIX—the multi-dimensional spectroscopy and inelastic x-ray scattering endstation," J. Phys. Condens. Matter **31**, 014003 (2019).

[43]G. Brenner, S. Dziarzhytski, P. S. Miedema, B. Rösner, C. David, and M. Beye, "Normalized single-shot x-ray absorption spectroscopy at a free-electron laser," Opt. Lett. **44**, 2157 (2019).

[44]R. Y. Engel, M. Ekimova, P. S. Miedema, C. Kleine, J. Ludwig, M. Ochmann, B. Grimm-Lebsanft, R. Ma, M. Teubner, S. Dziarzhytski, G. Brenner, M. K. Czwalinna, B. Rösner, T. K. Kim, C. David, S. Herres-Pawlis, M. Rübhausen, E. T. J. Nibbering, N. Huse, and M. Beye, "Shot noise limited soft x-ray absorption spectroscopy in solution at a SASE-FEL using a transmission grating beam splitter," Struct. Dyn. **8**, 014303 (2021).

[45]Atia-tul-noor, S. Kumar, N. Schirmel, B. Erk, B. Manschwetus, S. Alisaukas, M. Braune, G. Cirmi, M. K. Czwalinna, U. Frühling, U. Grosse-Wortmann, N. Kschuev, F. Kuschewski, T. Lang, H. Lindenblatt, I. Litvinyuk, S. Meister, R. Moshammer, C. C. Papadopoulou, C. Passow, J. Roensch-Schulenburg, F. Trost, I. Hartl, S. Düsterer, and S. Schulz, "Sub-50 fs temporal resolution in an FEL-optical laser pump-probe experiment at FLASH2," Opt. Express **32**, 6597 (2024).

[46]B. Lautenschlager, L. Butkowski, M. Czwalinna, B. Dursun, M. Hierholzer, S. Pfeiffer, H. Schlarb, and C. Schmidt, "Arrival time stabilization at flash using the bunch arrival corrector cavity (BACCA)," in *Proceedings of the 12th International Particle Accelerator Conference (IPAC2021)* (JACoW Publishing, 2021), p. 3.

[47]M. C. S. Schulz and H. Schlarb, "Latest achievements in femtosecond synchronization of large-scale facilities," in *13th International Beam Instrumentation Conference No. 13 (IBIC2024)* (JACoW Publishing, Geneva, Switzerland, 2024), pp. 457–464.
[48]T. Kachel, F. Eggenstein, and R. Follath, "A soft X-ray plane-grating monochromator optimized for elliptical dipole radiation from modern sources," J. Synchrotron Rad. **22**, 1301 (2015).
[49]W. Tang, C. Gerhards, J. Heise, and H. Zabel, "Structure and magnetic properties of $Fe_{1-x}Ni_x$/Cu Invar superlattices," J. Appl. Phys. **80**, 2327 (1996).
[50]More recent values of S_3 for the various photon energies have been provided by the beamline scientist at PM3 in a private communication.
[51]S. Mathias, C. La-O-Vorakiat, P. Grychtol, P. Granitzka, E. Turgut, J. M. Shaw, R. Adam, H. T. Nembach, M. E. Siemens, S. Eich, C. M. Schneider, T. J. Silva, M. Aeschlimann, M. M. Murnane, and H. C. Kapteyn, "Probing the timescale of the exchange interaction in a ferromagnetic alloy," Proc. Natl. Acad. Sci. U. S. A. **109**, 4792 (2012).
[52]C. von Korff Schmising, S. Jana, O. Zülich, D. Sommer, and S. Eisebitt, "Direct versus indirect excitation of ultrafast magnetization dynamics in FeNi alloys," Phys. Rev. Res. **6**, 013270 (2024).
[53]I. Radu, C. Stamm, A. Eschenlohr, F. Radu, R. Abrudan, K. Vahaplar, T. Kachel, N. Pontius, R. Mitzner, K. Holldack, A. Föhlisch, T. A. Ostler, J. H. Mentink, R. F. L. Evans, R. W. Chantrell, A. Tsukamoto, A. Itoh, A. Kirilyuk, A. V. Kimel, and T. Rasing, "Ultrafast and distinct spin dynamics in magnetic alloys," Spin **5**, 1550004 (2015).
[54]S. Marotzke, D. Gupta, R.-P. Wang, M. Pavelka, S. Dziarzhytski, C. von Korff Schmising, S. Jana, N. Thielemann-Kühn, T. Amrhein, M. Weinelt, I. Vaskivskyi, R. Knut, D. Engel, M. Braune, M. Ilchen, S. Savio, T. Otto, K. Tiedtke, V. Scheppe, J. Rönsch-Schulenburg, E. Schneidmiller, C. Schüßler-Langeheine, H. Dürr, M. Beye, G. Brenner, and N. Pontius (2025). "First experiments with ultrashort, circularly polarized soft X-ray pulses at FLASH2," Zenodo, Dataset. https://doi.org/10.5281/zenodo.15076836